Temperature-dependent Monte Carlo simulations of thin metal film growth and percolation

P. Bruschi, P. Cagnoni, and A. Nannini
Dipartimento di Ingegneria dell'Informazione: Elettronica, Informatica, Telecomunicazioni, Università degli Studi di Pisa, via Diotisalvi, 2 I56126 Pisa, Italy
(Received 25 October 1996)

A program for the simulation of the nucleation and growth of thin island films on amorphous substrates is presented. The program is based on the description of the phenomenon in terms of adsorption, diffusion, and reevaporation of single atoms on the substrate surface, which is represented as a triangular lattice of adsorption sites. A method of taking into account the interaction with neighboring particles in the evaluation of the diffusion activation barrier is proposed. The simulations are devoted to investigating the role of diffusion and reevaporation in the determination of the particular microstructure of the clusters. The effects of the substrate temperature on the morphology of the simulated island films are also presented. The cluster-size distribution and percolation threshold have been estimated and compared to experimental results available in the literature. [S0163-1829(97)05312-5]

I. INTRODUCTION

The early stages of the deposition of thin metal films onto amorphous substrates consists in the formation and growth of clusters that eventually connect each other to give a continuous percolating film. This process is of great importance for the properties of the final metal film, since the average grain size of polycrystalline films is affected by the size distribution of the clusters before the formation of a continuous phase.[1] The grain size, in turn, strongly affects the mechanical and electrical characteristics of the film: for example, the larger the grains, the higher the resistance to electromigration and therefore the longer the life of very large scale integration (VLSI) interconnections.[2]

Island metal films have also been studied for their intrinsic electrical properties[3–5] and applications as strain gauges have been proposed.[6] The charging-energy-limited tunneling model, which has successfully been applied to granular metals[7–9] and, subsequently, to conducting polymers,[10] was originally developed to explain the intriguing aspects of charge transport in island metal films.[3,4]

Recently, much interest has been raised by the percolative characteristics of thin island films.[11] In particular, the changes in morphology and size distribution of the metal clusters occurring when the percolation threshold is approached were investigated seeking analogies with the predictions of percolation theory. The power-law time dependence of the average grain size, predicted by the theory, was actually found by Xu *et al.* for copper, gold, and platinum ion-beam sputtered films.[12] The analysis of the cluster geometry at the percolation threshold, performed by Voss, Laibowitz, and Alessandrini[13] on gold thin films and by Kapitulnik and Deutscher[14] on Pb thin films, revealed a fractal dimensionality, as predicted by Monte Carlo simulations on percolative networks. However, the description given by percolation theory is limited only to a few properties of the cluster geometry that are independent of the experimental conditions: it does not take into account the microscopic mechanisms affecting the formation and rearrangements of the clusters and cannot therefore give any information on the effects of parameters such as the temperature on the structure of the island film.

The series of individual atomic processes occurring during the formation of a metal film are currently well understood.[15] The atoms arriving at the substrate from the source diffuse along the surface until they reevaporate or join other atoms to form clusters. Atoms belonging to clusters exhibit much less tendency to reevaporate but can still diffuse along the cluster borders causing cluster motion and rearrangement. Another process that can prevent reevaporation is capture of atoms by substrate defects. This model is the basis of the Zinsmeister kinetic rate equations, which has been used to describe the evolution of the cluster size distribution during the growth of a thin film in various experimental conditions.[15] A major limitation of this analytical approach is the fact that it cannot predict the shape of the clusters and therefore cannot be used to interpret phenomena, such as percolation of the metal phase, which are strongly dependent on the geometry of the clusters.

On the other hand, Monte Carlo simulations give much more information on the microstructure of the films and require only the knowledge of the atomic processes. A first example of computer simulation of the adsorption and diffusion of molecules on a surface is presented by Abraham and White[16] in the early 1970s. In this pioneering work the substrate is modeled as a square lattice of sites onto which the atoms impinge at a given rate; the adsorbed atoms can reevaporate or jump to a neighboring site (diffusion). The rate of these two processes is determined by a Boltzmann factor where the activation energy for reevaporation and diffusion of a given particle is calculated by summing up the energy of the broken bonds following the considered reevaporation or diffusion step. This simplified picture, which is also adopted by later works such as that of Salik,[17] conceals the much higher complexity of the potential experienced by a particle as a consequence of the interaction with its neighbors.

Starting from a Lennard-Jones approximation of the interatomic potential, Voter[18] calculated the total energy of a rhodium atom for all the possible occupancy of the neighbors and determined the activation barriers for hopping. The latter

was given by the energy of the saddle point of the total potential in the direction of hopping: for some configurations of the neighboring atoms the activation energy is significantly lower than that calculated with the broken bond criterion. A particularly important case is that of particles diffusing along the edge of clusters, since this is the mechanism by which clusters change shape and diffuse on the substrate.

Recently, the increasing computational power of today's computers, which allows the simulation of large arrays of atoms, has contributed to the rise in interest in Monte Carlo simulations of thin-film nucleation and growth. In particular, three-dimensional models capable of describing the behavior of few monolayers have appeared in the litterature. The transition from regimes of layer-by-layer and multilayer growth has been investigated, pointing out the role of additional energy barriers involved in atom's descending steps (Schwoebel barrier).[19,20] Such studies, mainly devoted to modeling molecular-beam-epitaxy deposition processes, deal with crystalline substrates that are easily represented by ordered arrays of sites. On the other hand, the substrates used in many deposition processes of practical interest are amorphous and, owing to the isotropy of their surface, do not have a straightforward lattice representation.

In this paper we present a program devised for the simulation of thin-film nucleation and growth on amorphous substrates. In order to limit the effects of anisotropy we have chosen to map the adsorption sites on a triangular lattice since it exhibits the higher degree of rotational symmetry. In addition, the activation energy associated to adatom hops is calculated by an algorithm that does not require a detailed knowledge of the strongly lattice-dependent interactions of the adatoms with the substrate and the neighbors but still allows one to distinguish the basic phenomena by which nucleation, diffusion, and reshaping of the clusters occur. In practice only two possible interactions with the neighbors, corresponding to (i) separation from one or more atoms, and (ii) motion along lines of atoms, are considered. In this way two values of energies, representative of atom departure from clusters and diffusion along the cluster edges, respectively, are sufficient for characterizing the dependence of the activation energy on the environment of the hopping particle. The algorithm is described in detail in Sec. III, where the effects of anisotropy on the diffusion of atoms along cluster edges are also pointed out. Although anisotropy is clearly unavoidable in a lattice representation, its effects on the simulated micrographs created by our program are much less relevant than those obtained by models specifically oriented to crystalline substrates.[19] The simulations are strictly two-dimensional, therefore only the submonolayer stage of growth can be represented. Island misorientation, typical of films grown onto amorphous substrates, is also not included in our simulations. This limitation leads to the concealment of grain boundary formation following coalescence of islands with different orientations.

The program has been optimized for handling large arrays of sites (up to 1000×1000), at high coverages: this involves a heavy computational load, especially for high temperatures where the rate of diffusion and reevaporation transitions increases. Furthermore, in order to get more reliable statistical data, we averaged the results of 10–20 simulations performed with different seeds for the random number generator. This results in the requirement of a high computational efficiency, which was achieved as a result of the simplicity of the algorithm for activation energy evaluation and the elimination of the waste of time due to null transitions by means of the method presented by Bowler and Hood[21] in their work on surface diffusion.

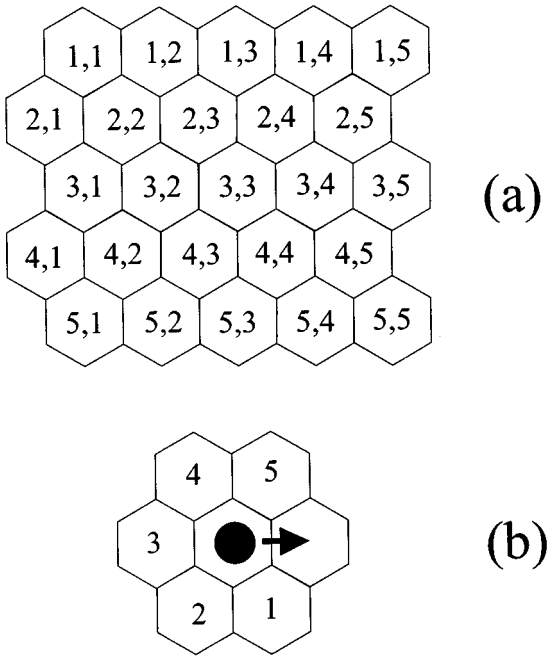

FIG. 1. Triangular lattice (a) of dimension 5×5 showing the method used to assign the coordinates to the sites; (b) symbolic representation of a particle hop, with the neighbors affecting the activation energy indicated by the numbers 1–5.

The aim of the program is to provide a tool for investigating the effects of the various elementary processes on the final structure of the islands. In particular, simulated micrographs and cluster-size distributions are created for different parameter settings and substrate temperatures in order to study the role of cluster edge diffusion and adatom reevaporation in determining the typical rounded shape of the clusters, observed in ultrathin metal films deposited onto amorphous substrates. The behavior of the percolation probability as a function of coverage and temperature is also presented, seeking correspondence with experimental data and simulations available in the literature.

II. MODEL OF SURFACE DIFFUSION AND FILM GROWTH

Three basic phenomena are considered: (i) adsorption of particles onto the substrate from the vapor phase, (ii) diffusion of particles on the substrate surface, and (iii) reevaporation from the substrate.

The substrate is modeled as a two-dimensional array of sites placed along a triangular lattice of lattice constant a. The criterion used to map the sites is shown for a 5×5 sample in Fig. 1(a), where the hexagonal Wigner-Seitz cells with their coordinates are drawn. The samples are of $N\times N$ type, corresponding to rectangles with dimensions $aN\times aN\sqrt{3}/2$.

Periodic boundary conditions were applied to the four extremes of the samples to reduce discontinuity. As a result: (i) a particle can move across one extreme and appear at the opposite one; (ii) particles placed at two opposite sides of the sample can be part of the same cluster.

At any step of the simulation, the program compiles a list of all the possible transitions of the system. The transitions can be divided into three groups, corresponding to the three basic processes listed above.

Group I includes a single transition, namely, the arrival of one particle at the substrate. The rate of this transition, r_a, is equal to the total number of particles arriving on the substrate per unit time. It is convenient to relate r_a to the quantity $R=r_a/N^2$, which gives the number of impinging particles per site and unit time.

The transitions of group II are all the allowed jumps of particles to their six nearest-neighboring sites. Only hops to vacant sites are allowed. Each one of the transitions of group II consists of the jump of only one particle at a time. The rate r_{ijkl} of the transition operated by particle in site i,j jumping to site k,l is defined by the expression

$$r_{ijkl}=r_0\exp\left(\frac{-E_{ijkl}}{kT}\right), \tag{1}$$

where E_{ijkl} is the activation energy of the transition and r_0 is a factor related to the vibrational frequency of the particle. Following the indications of Ref. 21 we neglect the dependence of r_0 in the neighborhood of the diffusing particle. The activation energy is determined by taking into account the occupancy of the nearest neighbors of the diffusing particle.

Group III includes all the transitions resulting from reevaporation of a single particle at a time. This is accomplished by removing the particle from the lattice. Clearly the number of transitions in group III is equal to the total number of particles in the sample. The rate of group III transitions is given by an expression similar to Eq. (1):

$$r_{ij}^{(e)}=r_0^{(e)}\exp\left(\frac{-E_{ij}^{(e)}}{kT}\right). \tag{2}$$

As in Eq. (1), $r_0^{(e)}$ is considered as a constant. $E_{ij}^{(e)}$ is the activation energy for reevaporation and is completely determined by the occupancy of the nearest neighbors of the particle. The algorithm used to calculate the activation energy in Eqs. (1) and (2) is described in the next section.

Each transition is represented by a record of the list; the records include all the information required to identify the transition, i.e., type I, II, or III, initial position of the particle (for types II and III only), hopping direction (for type II only), and rate.

At this point a transition is chosen and applied to the sample. This is done following the time-dependent Monte Carlo method of Ref. 21. Briefly, the transitions are arranged in sublists according to their rate. The occurrence frequency r_{si} of sublist i is given by the product

$$r_{si}=n_i r_i, \tag{3}$$

where r_i and n_i are the individual rate and total number of the transitions in sublist i. A probability proportional to their occurrence frequency is then assigned to the sublists and one of them is randomly chosen, according to these probabilities. Finally a transition is randomly chosen within the selected sublist with uniform probability over the whole sublist.

If the selected transition is a deposition event (group I transition) than a new particle is placed on the lattice at a site chosen randomly with uniform probability over the whole sample. If the chosen site is already occupied then a random walk is performed until an empty site is reached, since only two-dimensional simulations are currently available by the program.

At each step the time is increased by the transition time δt, given by the inverse of the sum of the rates of all the transitions. The latter is calculated by summing up the rates of all the sublists, obtaining for δt the expression

$$\delta t=\left(\sum_i r_{si}\right)^{-1}. \tag{4}$$

At the beginning of the simulation all the lattice sites are marked as empty.

III. DETERMINATION OF THE ACTIVATION ENERGY OF SURFACE DIFFUSION AND REEVAPORATION

Any given particle in the lattice can virtually cause seven distinct transition, i.e., hopping in six different directions and reevaporation. The rates of these transitions are related to activation barriers through Eqs. (1) and (2).

The activation energy for reevaporation is calculated as in Ref. 16 by the formula

$$E_{ij}^{(e)}=E_S^{(e)}+n_{ij}E_B, \tag{5}$$

where $E_S^{(e)}$ and E_B are, respectively, the binding energy of the particle with the substrate and with adjacent particles and n_{ij} is the number of filled nearest neighbors of the particle itself.

As far as hopping is concerned, the five neighbors affecting the transition [see Fig. 1(b)] are not treated in the same way but their position with respect to the hopping direction is taken into account. The activation energy is defined as a sum of contributions, one of which, E_S, is fixed and due to interaction with the substrate, the others derive from the interaction with filled neighbors. E_S is the diffusion activation energy of free particles, i.e., particles with no filled neighbors.

In order to understand the algorithm it is useful to start by considering a case with only one filled neighbor. If we put the particle in sites 2, 3, and 4 [Fig. 1(b)], then the hop results in a broken bond and the activation energy is the binding energy between particles, equal to E_B in Eq. (5). On the other hand, a particle in site 1 or 5 gives a contribution E_L related to the saddle point of the interatomic potential between the initial and final position.

For more than one filled site in the neighborhood, the program adds up the contributions of the single sites with the following two exceptions: (a) if site 1 is filled, then the contribution of site 2 is discarded; (b) if site 5 is filled, then the contribution of site 4 is discarded.

Figure 2 illustrates the activation energies for a few significant cases: in Figs. 2(a)–2(c) the single contributions can

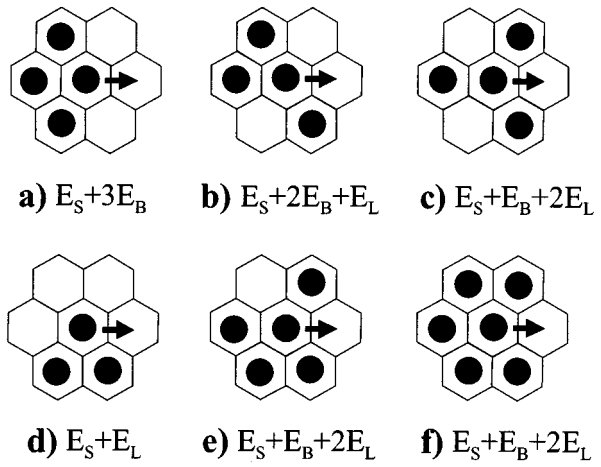

FIG. 2. Some examples of activation energy calculation. For the environments shown in (a)–(c) the contribution of the single neighbors are simply summed up while this does not apply to examples (d)–(f).

be simply added up while in Figs. 2(d)–2(f) this does not apply owing to the exceptions listed above.

The consequence of exception (a) and (b), which are symmetrical, is that a particle moving along a line of filled sites as shown in Fig. 3(a) experiences an activation barrier equal to E_L+E_S. Ideally, in a perfectly isotropic model, this should happen for lines of any direction, thus permitting one to relate the energy E_L to the activation barrier for particle migration along the perimeter of large regularly shaped clusters. In this ideal model, the energy E_B, related to the separation of two particles, affects only defect creation in perfect lines or departure of particles from clusters [Fig. 3(b)]. Actually, this holds true only for the three symmetrical directions equivalent to that of Fig. 3(a). In all the other cases, due to discretization, migration along lines of filled sites involves also steps with activation energy including the E_B contribution. The worst case is shown in Fig. 3(c), where for one step in every two the activation energy includes E_B.

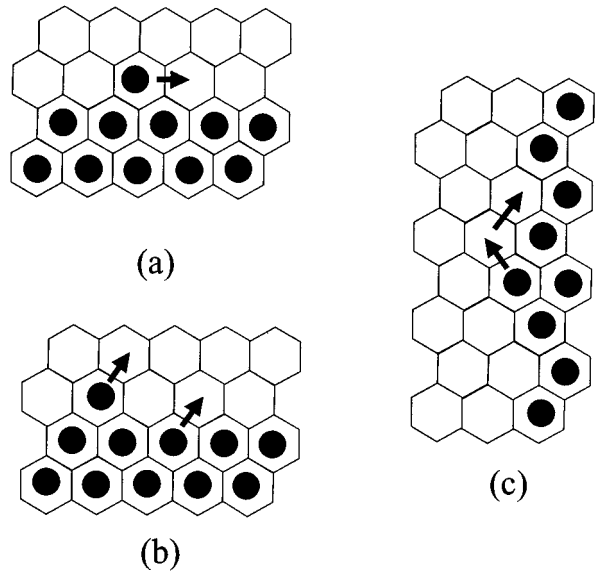

FIG. 3. Three significant cases of motion of atoms tied to the border of large clusters. (a) Diffusion along a straight line characterized by the minimum activation barrier; (b) hops resulting in particle departure from the cluster surface (left) or creation of a defect in a perfect line (right); (c) motion along a line involving also steps affected by a contribution to the activation energy due to broken bonds.

The algorithm is represented by the following formula, which gives the diffusion activation energy as a function of the occupancies c_1-c_5 of sites 1–5 in Fig. 1(b):

$$E_{ijkl}=E_S+(c_3+\overline{c_5}c_4+\overline{c_1}c_2)E_B+(c_1+c_5)E_L, \quad (6)$$

where the occupancy c_i of a given site is defined as 0 if the site is empty and 1 if it is filled and $\overline{c_i}=1-c_i$.

In order to improve the computational efficiency, a catalog including the transition rates for all the possible environments of a particle is compiled at the beginning of the simulation using Eqs. (1), (2), (5), and (6). The catalog is made up of 2^6 records, each one representing a configuration of the neighbors; the records include seven fields in which the rates of the possible transitions (hopping to the six neighbors and reevaporation) are stored. Transitions consisting of hopping to a filled neighbor are not allowed and are marked by setting the related rate in the catalog to a negative number.

During the simulation, every time the program needs to find the transitions associated to a particle and to calculate their rates, it takes these data from the catalog without performing floating point operations. The correspondence between the configurations of the neighbors and their related records has been studied to further speed up the simulations: the records are indexed according to a number whose binary digits are the occupancies of the ordered nearest neighbors.

IV. RESULTS

In this section we describe the results of a series of simulated depositions operated on 400×400 substrates. The experimental conditions are represented by nine physical quantities: the four energies E_S, $E_S^{(e)}$, E_B, E_L, the three rates r_0, $r_0^{(e)}$, R, the temperature T, and the deposition time t_d. It can be easily shown that this set is redundant and can be reduced to an equivalent set of seven dimensionless parameters consisting of the dimensionless temperature $T/T_0=k_BT/E_S$ the dimensionless time t_dr_0, and the ratios $E_S^{(e)}/E_S$, E_B/E_S, E_L/E_S, $r_0^{(e)}/r_0$, and R/r_0.

A first series of experiments was performed by varying the deposition temperature and the final fractional area coverages. The estimation of the parameters E_B/E_S and E_L/E_S requires the availability of data such as those reported by Voter in Ref. 18 for rhodium. To our knowledge, similar data for metals commonly used to grow island thin films (such as gold, copper, and platinum) are not available in the literature. In practice we have assigned the value 0.5 to E_B/E_S, which is related to separation of particles, and 0.2 to E_L/E_S, involved in the diffusion of particles along the perimeter of a cluster. The choice $E_B/E_S=0.5$ was made in conformity with the work of Voter; on the other hand, from the same work, a negative value for E_L/E_S can be extrapolated. The consequence is that free particles are less mobile than particles attached to the border of a cluster. We believe that this

is not the case of films grown onto amorphous substrates, which, especially for noble metals, exhibit an adhesion to the substrate smaller than cohesion. Therefore E_L/E_S was given a value significantly lower than E_B/E_S but still positive.

In this first series of simulations reevaporation has been inhibited by letting $r_0^{(e)}/r_0=0$. The deposition time $t_d r_0$ is fixed to 10^{15}. Fractional coverages in the range $0.15-0.7$ are obtained by varying the deposition rate R/r_0 in the range $(1.5-7)\times10^{-16}$. The effect of reevaporation is investigated by means of dedicated simulations described at the end of this section.

Figure 4 shows 100×100 portions of samples characterized by different fractional area coverage and substrate deposition temperature. At the lowest temperature, surface diffusion of particles and clusters is inhibited and the samples are very similar to random site percolation networks (RSPN) such as those reported by Smilauer in Ref. 11. As the temperature is raised, surface diffusion of single particles causes particle grouping into islands. It can be observed that the higher the temperature, the larger the islands. Also the island shape changes with the temperature. At the two intermediate temperature of Fig. 4, ''dendritic'' island growth occurs, in conformity with the results of Amar, Family, and Lam[22] concerning the simulation of molecular-beam-epitaxy depositions with a model that allows only free monomers to diffuse. In our model, when the temperature is high enough to activate particle diffusion along the cluster perimeters, the islands become more regularly shaped.

Observing that the transition from a dendritic island (DI) to a rounded island (RI) occurs at the absolute temperature $T_t=0.04\times T_0=0.04\times E_S/k_B$ (see Fig. 4) and referring to the activation energy of diffusion reported by Venables, Spiller, and Hanbücken,[15] it can be found that T_t should vary over the interval 37–200 K. This is consistent with transmission electron microscope observations of thin film grown at a substrate temperature greater than or equal to room temperature,[4,5,13,23,24] which are characterized by a RI structure. Dendritic island growth can be observed at low substrate temperature or in systems with higher activation energies of diffusion, such as homoepitaxial thin films.[22] The calculation of the effective deposition rate corresponding to the parameter R/r_0 requires the knowledge of the attempt frequency r_0: values of this quantity reported in the review paper by Venables, Spiller, and Hanbücken[15] range from 1.5×10^{10} sec^{-1} to 3.6×10^{13} sec^{-1}. Letting $r_0=10^{12}$ sec^{-1}, in conformity with Ref. 20, the resulting flux R of impinging atoms is in the interval $(1.5-7)\times10^{-4}$ atom sec^{-1}site^{-1}. Considering that the time required for the completion of a monolayer is equal to R^{-1}, and assuming an average spacing between successive monolayers of 0.4 nm, the effective deposition rates represented by our simulations fall in the range $(4-17)\times10^{-3}$ nm min^{-1}, depending on the selected final coverage x. These values are of the same order as those reported in Ref. 24 for ion-beam deposition of Au, Cu, Pt, and Ni at room temperature, resulting in films with a rounded island microstructure. No dendritic growth at similar deposition rates was also observed in Ref. 25 for Si deposited by molecular beam epitaxy onto silicon crystalline substrates at a temperature of 683 K.

The island diameter distribution is shown in Fig. 5 for various coverages and temperatures. The diameter of a cluster was defined as the longest line connecting two points of the cluster itself. For each coverage-temperature combination the distributions are averaged over ten samples, created using different seeds for the random number generator.

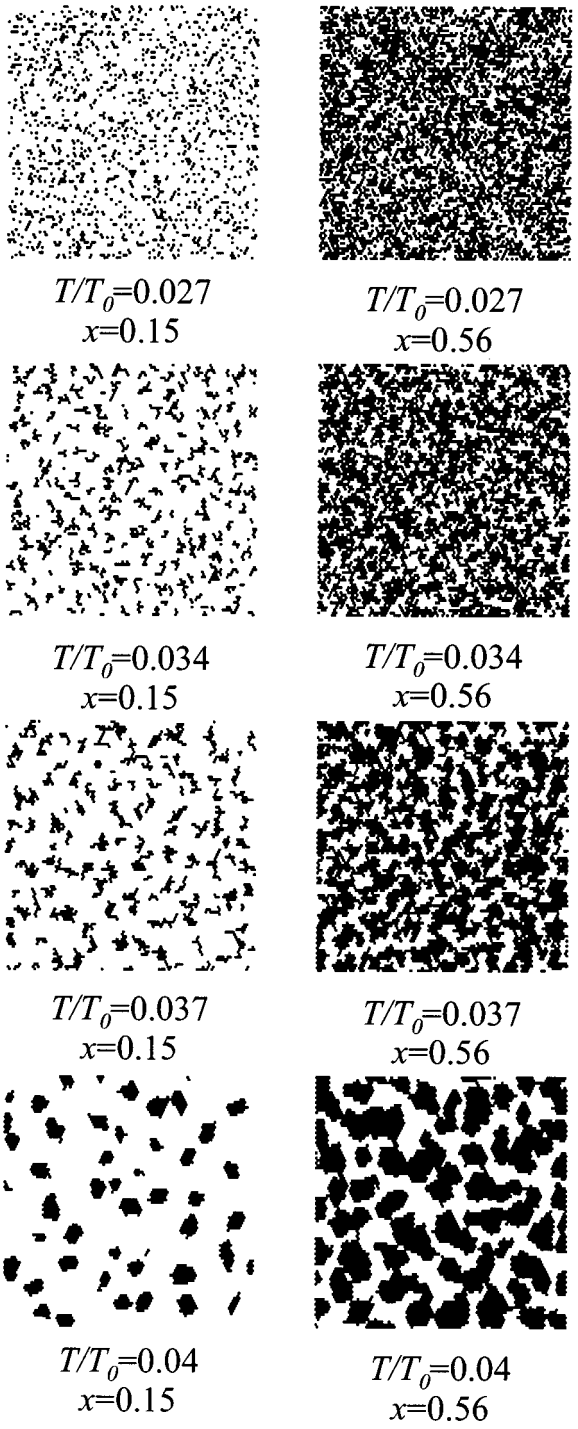

FIG. 4. Results of simulated depositions performed at different substrate temperature and final fractional coverages. The rate of reevaporation is set to zero. The figure shows 100×100 portions of 400×400 samples; the coverage (x) and normalized temperature (T/T_0) are indicated for each sample.

Samples created at low temperature (RSPN structure) exhibit monotonic distributions while for higher temperature a peak in the curves can be observed. This is consistent with

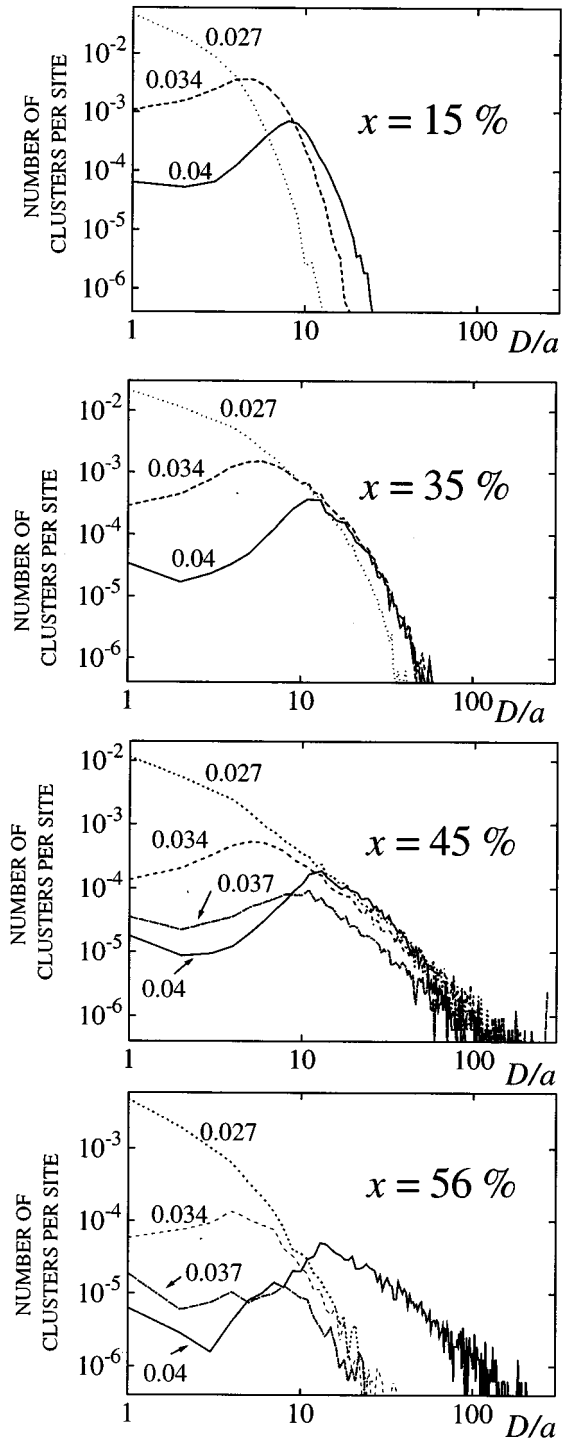

FIG. 5. Cluster size distributions for some significant coverages. The diameter (D) is normalized to the lattice constant (a). For each coverage the distributions relative to different settings of the substrate temperature are shown; the normalized temperature is indicated for each curve. The rate of reevaporation is set to zero.

the analytical description of the phenomenon reported in the review paper of Venables, Spiller, and Hanbücken:[15] in this case monotonic distributions are obtained by assuming cluster growth occurring by direct impingement of atoms (i.e., neglecting surface diffusion) while single-peaked distributions result from the assumption that clusters grow by coalescence processes due to surface diffusion of single particles or clusters. It should be noted that, in our model, switching from one regime to the other is a simple consequence of increasing the substrate temperature; furthermore, no additional hypothesis is needed to characterize cluster diffusion and coalescence, as both phenomena are due to the diffusion of single particles.

Single-peaked distributions were found in several experimental works[23,26–28] although the reported cluster density generally vanishes at the smallest cluster sizes. The discrepancy with the simulated distributions shown in Fig. 5 can be the result of the difficulty of detecting islands made up of very few atoms as suggested in Ref. 29.

The onset of a peak in the distribution is the consequence of the growth of large islands by incorporation of small mobile clusters impinging on their border In fact, as the temperature increases, the concentration of small clusters drops, while that of large clusters increases.

Figure 6 shows the percolation probability P_P as a function of the deposition temperature for three different coverages. The graphs represent the behavior of P_P calculated following two different definitions, applicable to finite lattices:[30] the first, indicated with IC (infinite cluster) is the ratio of the number of sites belonging to the infinite cluster (i.e., larger than the substrate) to the total number of filled sites; the second, indicated with CP (conducting path) is the fraction of samples that exhibit a path of filled sites between the right and left side of the substrate.

In all the three cases of Fig. 6 P_P falls to zero at the upper limit of the temperature interval. This is clearly the result of the reduction of island branching visible in Fig. 4. A less obvious result is the presence of a temperature interval in which the probability of creating a percolating sample is maximum. This behavior is emphasized at $x=0.45$ (see Fig. 6), where P_P is strictly zero except for a small interval around $T/T_0=0.037$. The cause is probably the activation of diffusion on the edge of the islands (activation energy, E_L+E_S), which creates links between large clusters. To our knowledge, this phenomenon has no experimental counterpart. To break the links, the temperature should be raised until separation of the particle is also allowed (activation energy, E_B+E_S).

In Fig. 7 the IC percolation probability has been plotted as a function of the fractional area coverage. At the lowest temperature the percolation threshold x_c is close to 0.5, which is its theoretical value for random site percolation in a triangular lattice.[31] At $T/T_0=0.037$ the percolation curve shifts back for the phenomenon of temperature-induced percolation illustrated in Fig. 6, at $x=0.45$. If the deposition temperature increases further, the percolation threshold increases, approaching 0.7 at $T/T_0=0.054$, as shown in Fig. 7. As we have seen before, in most thin-film deposition experiments the substrate temperature falls in the interval represented by $T/T_0>0.04$, and therefore we would expect high x_c values. Actually, while our results are in good agreement with the simulations of Amar and Family,[19] and experimental data reported in the literature,[13] x_c can assume values considerably higher for low melting point metals [up to 0.82 for In (Ref. 32) and Pb (Ref. 33) on amorphous SiO_2]. This is probably due to a three-dimensional growth of the clusters occurring during coaleascence with the result of freeing portions of substrate.[32]

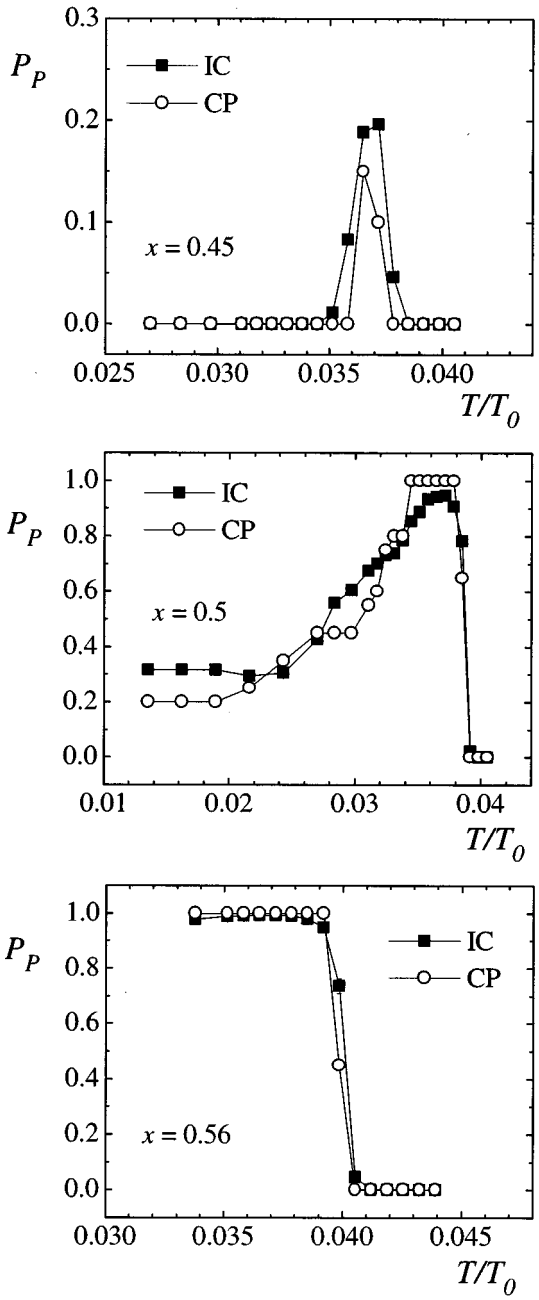

FIG. 6. Percolation probability (P_P) of 400×400 samples as a function of the normalized temperature for three values of coverage (x). For each covergage the percolation probability calculated with the infinite cluster (IC) and conducting path (CP) method are shown.

A second series of simulations was dedicated to studying the effect of reevaporation on the morphology of the films. Samples of dimensions 400×400 have been generated with $r_0^{(e)}/r_0=1$ while the ratio $E_S^{(e)}/E_S$ was varied in the range $0.9-2$. The normalized temperature was fixed to 0.034, a value at which surface diffusion alone is not sufficient to cause the transition to a RI structure. In Fig. 8 the microstructure of two samples of fractional coverage equal to 0.15 and 0.5, created with $E_S^{(e)}/E_S=0.9$, is shown. From the comparison with samples created at the same temperature and similar coverages (see Fig. 4) it can be observed that switching on reevaporation results in particle aggregation into large round clusters. This is a consequence of Eq. (5), which implies that the larger the number of adjacent particles the higher the activation barrier for reevaporation. Although Figs. 4 and 8 clearly demonstrate that a transition to a RI microstructure can be due to either reevaporation or particle diffusion along cluster edges, the resulting sample morphologies are different in the two cases as can be evidenced by inspection of the diameter distributions. In Fig. 9 the diameter distribution is shown for samples of coverage 0.15 and 0.5. The curves, averaged over sets of ten samples, refer to three different $E_S^{(e)}/E_S$ ratios; for $E_S^{(e)}/E_S>1.1$ the distributions are nearly identical and correspond to depositions with negligible reevaporation. A progressive shift towards a monotonic distribution can be observed as a consequence of the activation of reevaporation. On the other hand, a RI microstructure obtained through diffusion operated rearrangement of the clusters is marked by opposite changes in the distributions, namely, the onset of a peak as shown in Fig. 5. This is an important result, which provides a method to identify the origin of the RI microstructure through the analysis of the diameter distribution. As stated above, thin island

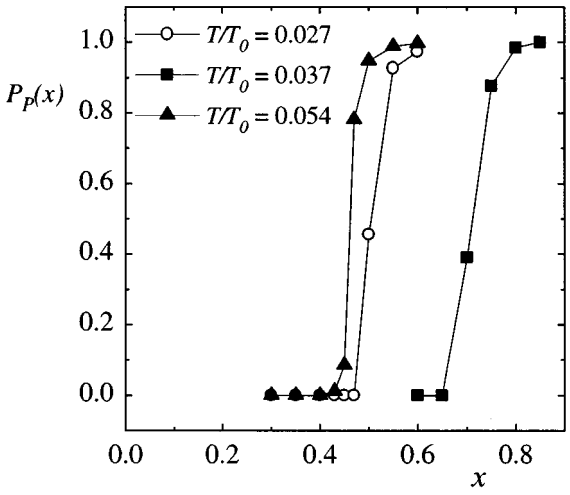

FIG. 7. Percolation probability, calculated with the infinite cluster method, plotted as a function of the fractional coverage for three significant normalized temperatures. Note the temperature dependence of the percolation threshold.

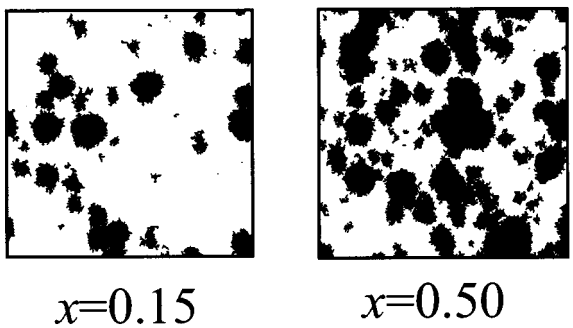

FIG. 8. Effect of reevaporation: the figure shows 200×200 portions of 400×400 samples created with the following setting: $E_S^{(e)}=0.9\times E_S$, $r_0^{(e)}=r_0$.

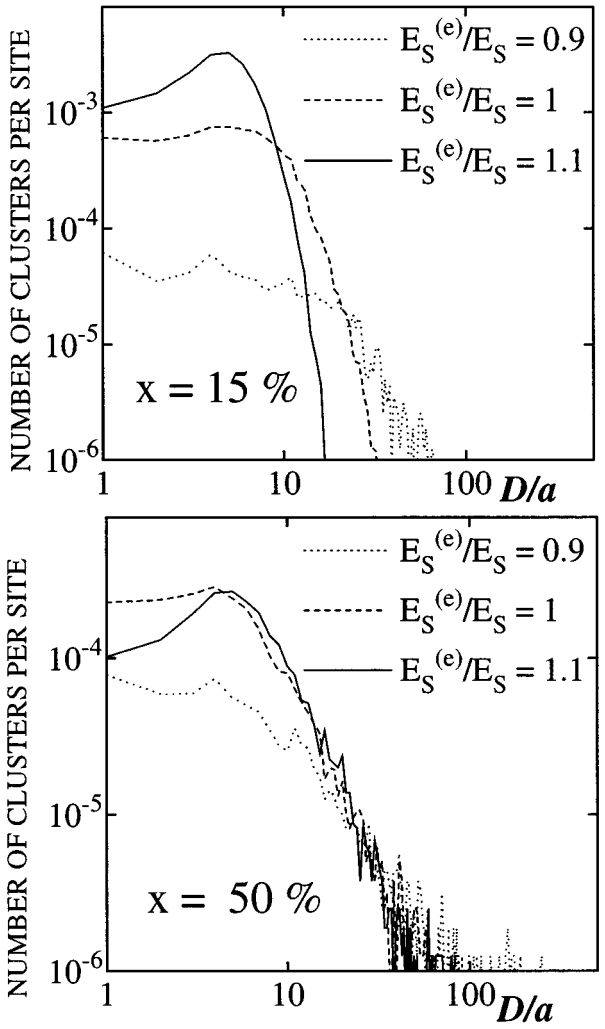

FIG. 9. Cluster diameter distributions relative to simulations performed with the same parameter setting of Fig. 8.

films are generally characterized by a peaked diameter distribution and rounded clusters. Following the criterion suggested by our simulations, it is possible to relate the formation of large rounded clusters to the diffusion of particles or smaller clusters on the substrate surface, ruling out reevaporation. In particular, diffusion of particles along the cluster borders plays a key role, being the mechanism by which cluster movement and rearrangement occurs.

V. CONCLUSIONS

The program described in this paper has been proven to be effective in describing the changes occurring in the microstructure of island films when the substrate temperature and the fractional coverage are varied over a wide interval.

Varying the dimensionless temperature kT/E_S and setting to zero the rate of reevaporation transitions, it has been shown that samples with three different structures can be generated: at temperatures low enough to freeze diffusion, the situation is that of a random site percolating network, with high density of small island; raising the temperature up to the activation of single adatom diffusion, larger islands with a very branched (dendritic) shape can be observed; finally, a further temperature increase activates diffusion along the border of the clusters and the islands become more regularly shaped. Referring to the values of E_S (the activation energy for single adatom diffusion) typically reported in the literature for metals, the dimensionless temperature at which the transition to rounded clusters occurs can be related to absolute temperatures significantly below room temperature. This is consistent with the micrographs of thin island films grown on amorphous substrates maintained at a temperature greater than or equal to room temperature showing clusters with very regular round shapes. The peaked cluster-size distribution and high percolation threshold typical of metal film grown in these conditions have also been predicted by the simulations. For its two-dimensional structure, the program is not applicable to the growth of metal films on nonwetting substrates, as in the case of Pb and In on SiO_2, in which the clusters consist of droplets with thicknesses of several monolayers. The simulation of such systems requires a three-dimensional model where, in order to take into account the thickness increase following the coalescence of two islands, adatoms should be allowed not only to descend terraces, as in crystalline-substrate oriented models, but also to climb steps. An extension of our model, aimed to include these three-dimensional mechanisms is in preparation.

Another process that could be responsible for cluster rearrangements towards a round shape is reevaporation of the adatom from the substrate, as clearly shown by a series of simulations performed with a parameter setting such as to freeze atom diffusion along cluster border and to activate reevaporation. However, different effects on the cluster size distribution can be observed in this case: reevaporation tends to produce monotonic size distribution curves, which can be easily distinguished from the strongly peaked distributions due to surface diffusion. Comparison with the typical cluster size distributions, estimated by analysis of transmission electron micrographs, suggests that the phenomenon responsible for island aggregation and rounding is atom diffusion along the border of the clusters while reevaporation does not play a significant role in metal film nucleation and growth.

[1] C. A. Neugebauer, in *Handbook of Thin Film Technology*, edited by L. E. Maissel and R. Glang (McGraw-Hill, New York, 1983).
[2] A. Scorzoni, B. Neri, C. Caprile, and F. Fantini, Mat. Sci. Rep. **7**, 143 (1991).
[3] C. A. Neugebauer and M. B. Webb, J. Appl. Phys. **33**, 74 (1962).
[4] R. M. Hill, Proc. R. Soc. London Ser. A **309**, 377 (1969).
[5] Z. H. Meiksin, Phys. Thin Films **8**, 99 (1975).
[6] G. R. Witt, Thin Solid Films **22**, 133 (1974).
[7] P. Sheng, B. Abeles, and Y. Arie, Phys. Rev. Lett. **31**, 44 (1973).
[8] C. J. Adkins, J. Phys. C **20**, 235 (1987).
[9] P. Bruschi, A. Nannini, and F. Massara, Thin Solid Films **196**, 201 (1991).

[10] H. Stubb, E. Punkka, and J. Paloheimo, Mat. Sci. Eng. **10**, 85 (1993).
[11] P. Šmilauer, Contemp. Phys. **32**, 89 (1991).
[12] S. Xu, B. L. Evans, D. I. Flynn, and C. En, Thin Solid Films **238**, 54 (1994).
[13] R. F.Voss, R. B. Laibowitz, and E. I. Alessandrini, Phys. Rev. Lett. **49**, 1441 (1982).
[14] A. Kapitulnik and G. Deutscher, Phys. Rev. Lett. **49**, 1444 (1982).
[15] J. A. Venables, G. T. D. Spiller, and M. Hanbücken, Rep. Prog. Phys. **47**, 399 (1984).
[16] F. F. Abraham and G. M. White, J. Appl. Phys. **41**, 184 (1970).
[17] J. Salik, Phys. Rev. B **32**, 1824 (1985).
[18] A. F. Voter, Phys. Rev. B **34**, 6819 (1986).
[19] J. G.Amar and F. Family, Thin Solid Films **272**, 208 (1996).
[20] M. Breeman, G. T. Barkema, M. H. Langelaar, and D. O. Boerma, Thin Solid Films **272**, 195 (1996).
[21] A. M. Bowler and E. S. Hood, J. Chem. Phys. **94**, 5162 (1991).
[22] J. G. Amar, F. Family, and P. M. Lam, Phys. Rev. B **50**, 8781 (1994).
[23] J. G. Skofronick and W. B. Phillips, J. Appl. Phys. **38**, 4791 (1967)
[24] S. Xu and B. L. Evans, J. Mater. Sci. **27**, 3108 (1992).
[25] L. Andersohn, T. Berke, U. Köhler, and B. Voigtländer, J. Vac. Sci. Technol. A **14**, 312 (1996).
[26] J. A. Blackman, B. L. Evans, and A. I. Maaroof, Phys. Rev. B **49**, 13 863 (1994).
[27] G. Fuchs, D. Neiman, and H. Poppa, Thin Solid Films **207**, 65 (1992).
[28] D. Beysens, C. M. Knobler, and H. Schaffar, Phys. Rev. B **41**, 9814 (1990).
[29] K. Kinosita, Thin Solid Films **85**, 223 (1981).
[30] B. S. Shklovskii and A.L. Efros, *Electronic Properties of Doped Semiconductors* (Springer, Berlin, 1994).
[31] V. K. S. Shante and S. Kirkpatrick, Adv. Phys. **20**, 325 (1971).
[32] X. Yu, P. M. Duxbury, G. Jeffers, and M. A. Dubson, Phys. Rev. B **44**, 13 163 (1991).
[33] G. Jeffers, M. A. Dubson, and P. M. Duxbury, J. Appl. Phys. **75**, 5016 (1994).